Orthorhombic carbon allotrope of compressed graphite: *Ab initio* calculations

Jian-Tao Wang,[1,*] Changfeng Chen,[2] and Yoshiyuki Kawazoe[3,4]

[1]*Beijing National Laboratory for Condensed Matter Physics, Institute of Physics, Chinese Academy of Sciences, Beijing 100190, China*

[2]*Department of Physics and High Pressure Science and Engineering Center, University of Nevada, Las Vegas, Nevada 89154, USA*

[3]*Institute for Materials Research, Tohoku University, Sendai 980-8577, Japan*

[4]*Kuwait Institute for Scientific Research, Safat, 13109, Kuwait*

(Received 22 December 2011; published 27 January 2012)

We identify by *ab initio* calculations an orthorhombic carbon (O-carbon) in $Pbam$ (D_{2h}^9) symmetry for compressed graphite in AA stacking, which is formed via a distinct one-layer by one-layer slip and buckling mechanism along the [210] direction. It is dynamically stable and energetically more favorable than other known compressed graphite phases, albeit its slightly higher kinetic barrier. The O-carbon is comparable to diamond in ultralow compressibility, has a band gap wider than that of diamond, and is compatible with experimental x-ray diffraction data. The present results offer insights for understanding the complex structural landscape of compressed graphite and the versatile nature of carbon in forming a rich variety of structures under pressure.

DOI: 10.1103/PhysRevB.85.033410 PACS number(s): 61.50.Ks, 61.66.Bi, 62.50.−p, 63.20.D−

Graphite transforms into hexagonal and cubic diamond under high-pressure and high-temperature conditions.[1–5] The phase transformation process is highly complicated and remains poorly understood despite extensive past effort. Compressed graphite acts as a key gateway toward various diamond phases; an accurate mapping of its structural landscape is essential to understanding the intricate phase relations among various carbon allotropes. Experimentally, an unquenchable transparent and hard phase has long been observed during the cold-compression (at room temperature) stage of the synthesis.[6–12] Recent studies have identified several structural forms for cold-compressed graphite, including a monoclinic M-carbon[13] and an orthorhombic W-carbon,[14] which provide a critical link for the graphite-to-diamond transformation.[15] However, graphite's layered structure is conducive to the sliding and buckling of the graphitic sheets during the initial stages of compression, which introduces a high degree of complexity in the structural landscape of compressed graphite.

In this Brief Report, we identify by *ab initio* calculations an orthorhombic carbon (O-carbon) allotrope in $Pbam$ (D_{2h}^9) symmetry, which is formed via a one-layer by one-layer slip and buckling along the [210] direction. This transformation mechanism is distinct from mechanisms previously proposed for M- and W-carbon that occur along the [100] direction.[14] Phonon calculations indicate that this phase is dynamically stable. Its simulated x-ray diffraction pattern matches well the experimental data on compressed graphite.[11] The O-carbon has a band gap wider than that of diamond and a bulk modulus comparable to that of diamond. It is more stable than W- and M-carbon energetically, although it has a slightly higher kinetic barrier. These results broaden our understanding of the complex structural landscape of compressed graphite and provide insights into the relations among the rich variety of carbon allotropes.

The calculations were carried out using the density functional theory within the local density approximation (LDA) as implemented in the Vienna *ab initio* simulation package (VASP).[16] The all-electron projector augmented wave (PAW) method[17] was adopted with $2s^2 2p^2$ treated as valence electrons. A plane-wave basis set with an energy cutoff of 800 eV was used, leading to well-converged total energy of ∼1 meV per atom. Forces on the ions were calculated through the Hellmann-Feynman theorem allowing a full geometry optimization. Band structures were calculated using the hybrid functionals (HSE06).[18] Phase transitions were simulated using the climbing image nudged elastic band method.[19] Phonon dispersion curves are calculated using the package MedeA (Ref. 20) with the forces calculated with the VASP.

The crystal structure of O-carbon with the space group $Pbam$ (D_{2h}^9) is shown in Fig. 1(a). It can be considered as distorted graphite in an AA stacking. At zero pressure, the equilibrium lattice parameters are $a = 4.755$ Å, $b = 7.786$ Å, and $c = 2.494$ Å with four inequivalent crystallographic sites, occupying the 4h (0.1072, 0.0706, 0.5), 4h (0.3614, 0.9546, 0.5), 4g (0.9632, 0.8267, 0.0), and 4g (0.3090, 0.8436, 0.0) positions, respectively. By fitting the calculated total energy as a function of volume to the third-order Birch-Murnaghan equation, we obtain the bulk modulus (B_0) of 438.6 GPa for O-carbon, which is larger than that of c-BN (396 GPa)[21] and very close to the value for W-carbon (445 GPa), M-carbon (439 GPa), and diamond (466 GPa) (see Table I). At high pressures, O-carbon becomes stable relative to graphite above 11.15 GPa [Fig. 1(a)], and it is more stable (i.e., lower in enthalpy) than both M-carbon[13] and W-carbon.[14] It is noted that the odd-membered-ring (5 + 7) connecting structures in M, W, and O-carbon are more favorable than the even-membered-ring (4 + 8) connecting structure in the bct-C_4 structure.[22]

Figure 1(c) shows the calculated band structure of O-carbon at 15 GPa using the hybrid functionals (LDA-HSE06)[18] that produce the band gap in good agreement with experimental data for diamond (see Table I). The valence band top and the conduction band bottom of O-carbon are both at the Γ point; the calculated band gap is 5.87−6.04 eV over a wide pressure range of 0–25 GPa, which is close to 5.69 eV for W-carbon, but markedly larger than 4.78 eV for M-carbon; it is even appreciably larger than the gap (5.43 eV) for diamond. Therefore, O-carbon is expected to be optically transparent like M-carbon and W-carbon. We have also calculated its phonon dispersion curves over a wide pressure range up to

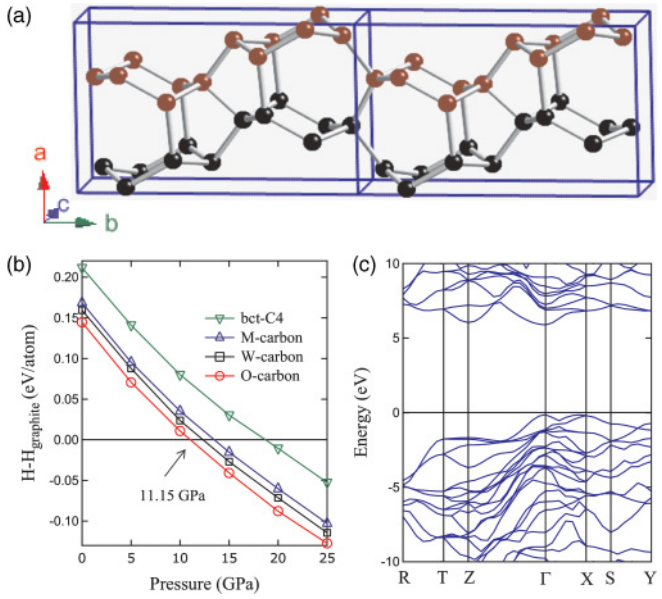

FIG. 1. (Color online) The orthorhombic O-carbon in $Pbam$ symmetry. (a) A polyhedral view of the crystal structure. (b) The enthalpy per atom (relative to that of graphite) for bct-C_4,[22] M-carbon,[13] W-carbon,[14] and O-carbon versus pressure. (c) Calculated electronic band structure of O-carbon at 15 GPa.

60 GPa. No imaginary frequencies were observed throughout the entire Brillioun zone, confirming the dynamical stability of the O-carbon phase.

Figure 2 shows the simulated x-ray diffraction (XRD) patterns of graphite, M-carbon, W-carbon, and O-carbon, compared to the experimental data at various pressure values.[11] Here the strongest peaks between 8.5° and 10.5° reflect the sp^3 bonding environment as in diamond,[15] while the peaks between 6° and 7° reflect the sp^2 bonding environment as in graphite. The XRD patterns of O-carbon are very similar to those of M-carbon in the region between 8.5° and 10.5° and to those of W-carbon in the region between 15° and 17°, which correspond almost exactly to where pressure-induced broad peaks appear in the experimental data.[11] These results

TABLE I. Calculated equilibrium volume (V_0 in Å^3/atom), bulk modulus (B_0 in GPa), and band gap (E_g in eV) for diamond, M-carbon, W-carbon, and O-carbon at zero pressure, compared to available experimental data[24] for diamond and calculated data for M-carbon[13] and W-carbon.[14]

Structure	Method	V_0 (Å^3)	B_0 (GPa)	E_g (eV)
Diamond	LDA[14]	5.52	466.3	4.20
	LDA[23]			4.17
	HSE			5.43
	Exp[24]	5.67	446	5.47
M-carbon	LDA[14]	5.79	438.7	3.56
	LDA[13]	5.78	431.2	3.60
	HSE			4.78
W-carbon	LDA[14]	5.76	444.5	4.39
	HSE			5.69
O-carbon	LDA	5.77	438.6	4.54
	HSE			5.87

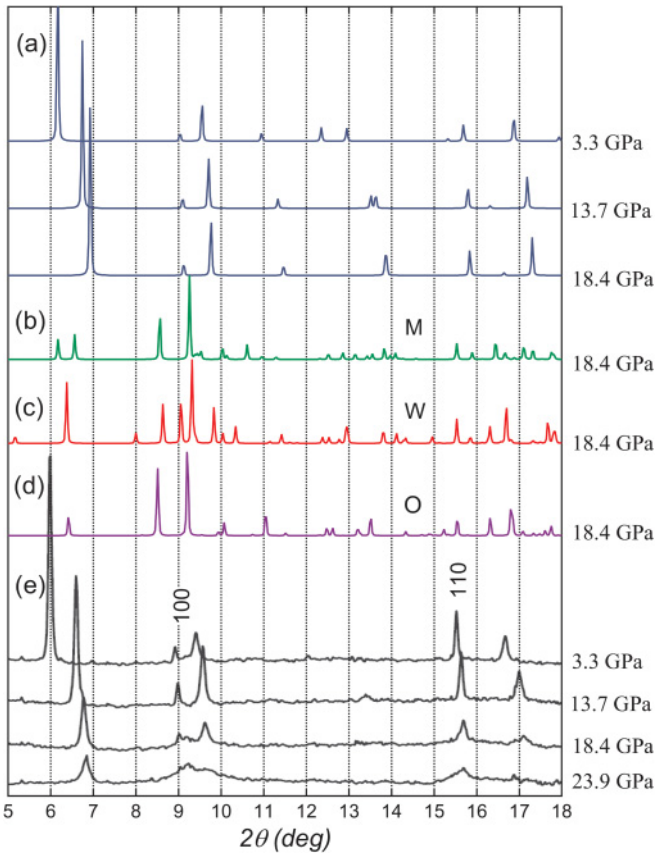

FIG. 2. (Color online) Simulated XRD patterns of (a) graphite at 3.3, 13.7, and 18.4 GPa and (b–d) M-carbon, W-carbon, and O-carbon, respectively, at 18.4 GPa. (e) Experimental XRD patterns.[11] The x-ray wavelength is 0.3329 Å.

suggest that O-carbon is among the likely candidates for the cold-compressed graphite phases.

We now study the atomistic processes underlying the transformation pathways from hexagonal graphite (hex-g) toward the O-carbon. These pathways are simulated using the CI-NEB method[19] with a 16-atom supercell containing two carbon sheets. No symmetry constraint was imposed in the structural optimization procedure. In contrast to the c-axis compression process from graphite to M- or W-carbon along the orientation a[100] of graphite,[14] here we identify a strong in-plane anisotropic compression pathway along the orientation b[210] of graphite with the lattice distortion from (a,b,c = 2.445 Å, 8.463 Å, 6.467 Å, respectively) for graphite to (a,b,c = 2.494 Å, 7.786 Å, 4.755 Å, respectively) for O-carbon. We find that the orthorhombic O-carbon is formed by alternating armchair buckling of the C_6 benzene rings (Fig. 3) via a one-layer (A) by one-layer (B) slip model along the [210] orientation. At the first stage (from step 0 to 33), two carbon sheets in AB stacking [Fig. 3(a)] slip relative to each other with a local buckling of the carbon sheets toward the formation of an intermediate cold-compressed graphite phase in AA stacking [Fig. 3(d)] with the cross-linking of half of the carbon atoms between the adjacent graphite sheets. Such cross-linking behavior agrees with the result of molecular dynamics simulations.[25] This compressed graphite phase consists of 10-membered rings in $Cmmm$ (D_{2h}^{19}) symmetry. However,

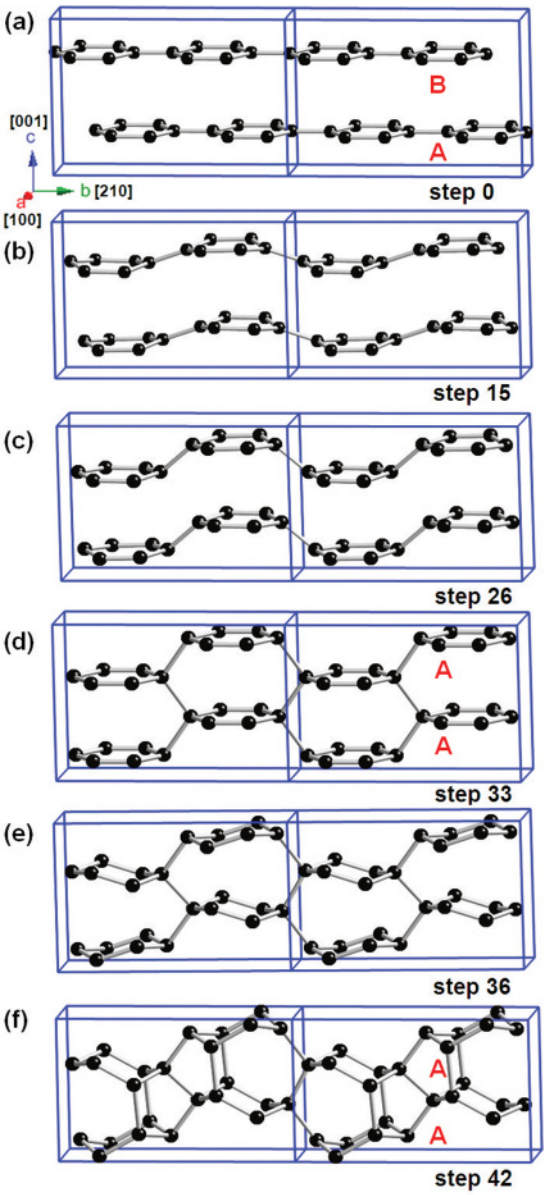

FIG. 3. (Color online) The slip and buckling phase conversion process from graphite toward O-carbon at 15 GPa along the [210] orientation of graphite. (a) Graphite in AB stacking shown as a rectangular supercell in $P63/mmc$ (No. 194) symmetry. (b,c) Structures at steps 15 and 26 along the pathway with a buckling carbon sheet in $Pbam$ (No. 55) symmetry. (d) Structure at step 33 in $Cmmm$ (No. 65) symmetry, consisting of the 10-membered rings with the cross-linking of carbon atoms between adjacent graphite sheets. (e) Structure at step 36 with a local distortion of the benzene rings in $Pbam$ (No. 55) symmetry. (f) The O-carbon in $Pbam$ (No. 55) symmetry shown as distorted graphite in AA stacking.

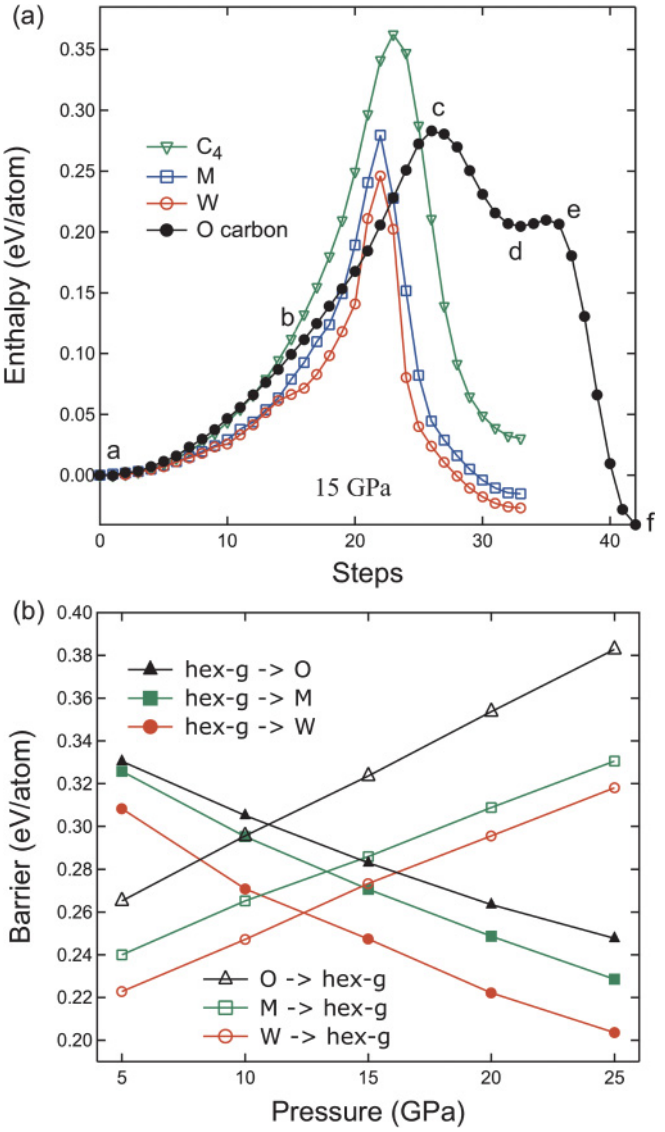

FIG. 4. (Color online) (a) Enthalpy versus pathway at 15 GPa. The letters a, b, c, d, e, and f refer to the images along the transformation pathway from graphite toward O-carbon shown in Fig. 3. The results for the bct-C_4, M-carbon, and W-carbon[14] are also shown for comparison. (b) Enthalpy barriers versus pressure. The solid and open symbols represent the reaction and counterreaction barriers, respectively.

such 10-membered ring structures are unstable in energy [see Fig. 4(a)]. In the ensuing second stage (from step 33 to 42), it converts to the (5 + 7)-membered rings to form O-carbon with a local distortion of the benzene rings [Fig. 3(e)].

Figure 4(a) shows the enthalpy along the pathway toward the formation of O-carbon at 15 GPa. Graphite's layered structure makes the buckling of the the graphitic sheets relatively easy to occur at the early stages of the transformation under compression. With the local bond rotation of the benzene rings, the enthalpy increases quickly due to bond twisting; then the enthalpy decreases with the cross-linking of the benzene rings between adjacent layers. The peak barrier occurs during the first-stage slipping process, and there is no energy cost during the second stage from the 10-membered ring structure to the sp^3 (5 + 7)-membered ring structure.

We compare the results for O-carbon with those for M- and W-carbon[14] and bct-C_4.[22] A close examination reveals that the pathway toward O-carbon is appreciably lower than that toward bct-C_4 and competitive with the pathways toward W- and M-carbon, although the latter two have lower enthalpy during the initial stages of compression. As a result, transformations

toward W- and M-carbon may be favored to initiate and proceed under a compression along the [001] direction. These results suggest that the transformation of cold-compressed graphite strongly depends on the compression direction; the O-carbon can be obtained under an anisotropic compression along the b[210] direction of graphite. It highlights the rich variety of transformation mechanisms for compressed graphite, which are sensitive to loading conditions.

Figure 4(b) shows that, with increasing pressure from 5 to 25 GPa, the barriers decrease from 0.331 to 0.248 eV for hex-g $\rightarrow O$-carbon, which is similar to the results for hex-g $\rightarrow M$-carbon and hex-g $\rightarrow$ W-carbon.[14] Pressure plays a key role in lowering the kinetic barrier and facilitates the phase transformation. Experimentally, the sp^3-bonded *transparent phase* of carbon is reversible with release of pressure at room temperature.[1,6,9,11] With decreasing pressure from 25 to 5 GPa, the counterreaction barriers are reduced from 0.383 to 0.265 eV for O-carbon $\rightarrow$ hex-g, which follows the same trend for M-carbon $\rightarrow$ hex-g and W-carbon $\rightarrow$ hex-g. These results underscore the key role of pressure in stabilizing O-carbon as well as W- and M-carbon under compression. We further studied the transformation of O-carbon to diamond structures and found that the path toward cubic diamond has the lowest barrier. This opens a pathway for graphite-to-diamond transition since W- and M-carbon tend to transform to 12R and hexagonal phases of diamond, respectively.[15]

In summary, we have identified a carbon allotrope in $Pbam$ (D^9_{2h}) symmetry for compressed graphite using *ab initio* calculations. We reveal an atomistic transformation mechanism along the [210] direction of graphite, which is distinct from the sliding-buckling mechanism along the [100] orientation for the recently identified orthorhombic W- and monoclinic M-carbon phases. These results advance our knowledge about the complex structural landscape of compressed graphite and the transformations among different carbon allotropes under diverse loading conditions.[26]

This study was supported by the NSFC (Grant No. 10974230) and the CAS (Grant No. KJCX2-YW-W22). C.F.C. is supported by the DOE (DE-FC52-06NA27684). Acknowledgment goes to the CREST Project headed by M. Kotani. We are thankful to the crew of the Center for Computational Materials Science at IMR, Tohoku University, for their support at the SR11000 supercomputing facilities.

*wjt@aphy.iphy.ac.cn

[1] F. P. Bundy and J. S. Kasper, J. Chem. Phys. **46**, 3437 (1967).
[2] R. Clarke and C. Uher, Adv. Phys. **33**, 469 (1984).
[3] T. Irifune, A. Kurio, S. Sakamoto, T. Inoue, and H. Sumiya, Nature (London) **421**, 599 (2003).
[4] H. Sumiya and T. Irifune, J. Mater. Res. **22**, 2345 (2007).
[5] F. P. Bundy, W. A. Bassett, M. S. Weathers, R. J. Hemley, H. K. Mao, and A. F. Goncharov, Carbon **34**, 141 (1996).
[6] E. D. Miller, D. C. Nesting, and J. V. Badding, Chem. Mater. **9**, 18 (1997).
[7] W. Utsumi and T. Yagi, Science **252**, 1542 (1991).
[8] M. Hanfland, K. Syassen, and R. Sonnenschein, Phys. Rev. B **40**, 1951 (1989).
[9] T. Yagi, W. Utsumi, M. A. Yamakata, T. Kikegawa, and O. Shimomura, Phys. Rev. B **46**, 6031 (1992).
[10] Y. X. Zhao and I. L. Spain, Phys. Rev. B **40**, 993 (1989).
[11] W. L. Mao, H. K. Mao, P. J. Eng, T. P. Trainor, M. Newville, C. C. Kao, D. L. Heinz, J. F. Shu, Y. Meng, and R. J. Hemley, Science **302**, 425 (2003).
[12] M. Hanfland, H. Beister, and K. Syassen, Phys. Rev. B **39**, 12598 (1989).
[13] Q. Li, Y. M. Ma, A. R. Oganov, H. B. Wang, H. Wang, Y. Xu, T. Cui, H. K. Mao, and G. T. Zou, Phys. Rev. Lett. **102**, 175506 (2009).
[14] J. T. Wang, C. F. Chen, and Y. Kawazoe, Phys. Rev. Lett. **106**, 075501 (2011).
[15] J. T. Wang, C. F. Chen, and Y. Kawazoe, Phys. Rev. B **84**, 012102 (2011).
[16] G. Kresse and J. Furthmüller, Phys. Rev. B **54**, 11169 (1996); G. Kresse and J. Hafner, Phys. Rev. B **47**, 558 (1993).
[17] P. E. Blöchl, Phys. Rev. B **50**, 17953 (1994); G. Kresse and D. Joubert, Phys. Rev. B **59**, 1758 (1999).
[18] A. V. Krukau, O. A. Vydrov, A. F. Izmaylov, and G. E. Scuseria, J. Chem. Phys. **125**, 224106 (2006).
[19] See [http://theory.cm.utexas.edu/henkelman].
[20] K. Parlinski, Z.-Q. Li, and Y. Kawazoe, Phys. Rev. Lett. **78**, 4063 (1997).
[21] A. F. Goncharov, J. C. Crowhurst, J. K. Dewhurst, S. Sharma, C. Sanloup, E. Gregoryanz, N. Guignot, and M. Mezouar, Phys. Rev. B **75**, 224114 (2007).
[22] K. Umemoto, R. M. Wentzcovitch, S. Saito, and T. Miyake, Phys. Rev. Lett. **104**, 125504 (2010).
[23] W. G. Aulbur, M. Stadele, and A. Gorling, Phys. Rev. B **62**, 7121 (2000).
[24] F. Occelli, P. Loubeyre, and R. Letoullec, Nat. Mater. **2**, 151 (2003).
[25] S. Scandolo, M. Bernasconi, G. L. Chiarotti, P. Focher, and E. Tosatti, Phys. Rev. Lett. **74**, 4015 (1995).
[26] Z. Zhao, B. Xu, X. F. Zhou, L. M. Wang, B. Wen, J. He, Z. Liu, H. T. Wang, and Y. Tian, Phys. Rev. Lett. **107**, 215502 (2011).